A POINT BASED NON-RIGID REGISTRATION FOR TUMOR RESECTION USING IMRI

Yixun Liu[1]*, Chengjun Yao*[2]*, LiangFu Zhou*[2]*, Nikos Chrisochoides*[1]

[1] Department of Computer Science, College of William and Mary, Williamsburg, USA
[2] Neurosurgery, Huashan Hospital, Shanghai, China

ABSTRACT

This paper presents a novel feature point based non-rigid registration of preoperative MRI with resected intra-operative MRI (iMRI) to compensate for brain shift during tumor resection.

The registration is formulated as a three variables (*Correspondence*, *Deformation Field* and *Resection Region*) functional minimization problem. We solve this problem by means of a nested Expectation and Maximization (EM) framework where: (1) the inner EM loop computes the *Correspondence* and *Deformation Field* by iteratively rejecting point outliers and (2) the outer EM loop computes the *Resection Region* by iteratively rejecting resected elements.

Our preliminary data from both synthetic and real brain MRI show the effectiveness of this method to handle tumor resection. The results of the registration in the vicinity of the tumor resection is on average, 16 times more accurate than the results from rigid registration.

Index Terms— Tumor Resection, Non-rigid registration, Outliers, Expectation and Maximization, Biomechanical Model.

1. INTRODUCTION

Although the maximum Non-Rigid Registration (NRR) error in the clinical studies [1] is improved on average by about four times compared to rigid registration, we observe that *the error is most significant in the vicinity of the tumor resection region —the place where high accuracy is needed the most.*

During the procedure, as part of the tumor is resected, the deformation induced by the resection will compromise the fidelity of the Image-Guided Surgery (IGS). The NRR, which takes the resected region into account, needs to be performed to compensate for the deformation. Very few studies in the literature address brain deformation during and after tissue resection. The difficulty originates from the fact that resection creates a cavity, which will change the domain on which the biomechanical model is defined. It is challenging to determine this cavity because portion of it will be filled by surrounding tissues [2].

Vigneron et al. [3] used the extended finite element method (XFEM) to model surgical cuts, retractions and resections. XFEM eliminates the computationally-expensive remeshing for the standard finite element method (FEM). The experiment on the simulation of 2D retraction demonstrated the effectiveness of this method.

THIS WORK IS SUPPORTED IN PART BY NSF GRANTS: CCF-0916526, CCF-0833081, AND CSI-719929 AND BY THE JOHN SIMON GUGGENHEIM FOUNDATION.

Miga et al. [4] investigated tissue retraction and resection using sparse available data in the operating room and finite element model. They use a two step method: (1) remove tissue volume by manual deletion of model elements that coincide with the targeted zone and then (2) apply boundary conditions to the new surfaces created during the excision process. Our method eliminates the manual removal step by treating the resected elements as outliers which are automatically rejected using an Expectation and Maximization (EM) framework [5].

Based on the bijective Demons algorithm, Risholm et al. in [6] presented a registration framework to handle retraction and resection. They used a level set method to automatically detect resected regions. Also, in [7], they presented an elastic FEM-based registration algorithm, but it is limited to registration of 2D pre- with intra-operative images, where a superficial tumor has been resected. We focus on 3D real pre- and intra-operative MRI data. Our method detects resected regions using an EM framework and only depends on a single parameter: threshold of the background.

Ding et al. [2] presented a semi-automatic method based on postbrain tumor resection and laser range data. Vessels are identified in both pre-operative MRI and laser range image; then the Robust Point Matching (RPM) method [8] is used to force the corresponding vessels to exactly match each other under the constraint of the bending energy of the whole image. RPM uses Thin-Plate Splines (TPS) as mapping function. However, TPS's basis functions do not have compact support, which leads to unrealistic deformation in the region far away from the matching points. In other words, RPM is not suitable for estimating deformation using sparse intra-operative data. Moreover, they do not consider changes in the bending energy (regularization term) introduced by tissue removal from the brain. Our work is addressing these two issues.

Periaswamy et at. [9] presented an intensity based registration with partial data. However, partial or incomplete data do not have the same meaning in the presence of a resection. The former means that a portion of the data is not visible, but still exists in the pre-operative MRI. In contrast, the latter means some portion is removed and thus the effect (i.e., contribution) of the stiffness in biomechanical model defined on resected region will not be considered. Biomechanical model based methods can deal with the partial data effectively because they rely on boundary conditions or sparse data for the solution. Although, the work in [9] is not directly related to tumor resection, the use of the EM method for solving two interdependent models motivates our nested EM framework.

2. METHOD

Given, $S = \{s_i\}_{i=1}^N \in \Re^3$ and $T = \{t_i\}_{i=1}^N \in \Re^3$, a *Source* and *Target* point set, respectively, we define the following minimization problem:

$$u = \underset{u}{\operatorname{argmin}} \left(\int_\Omega R(u) d\Omega + \lambda \sum_{s_i \in \Omega} \|s_i + u(s_i) - t_i\|^2 \right) \quad (1)$$

where the first term is regularization or smoothing term and the second term is similarity term. u is the deformation field with respect to the position and λ is used to control a trade-off between these two energies. Ω is the problem domain, more specifically the brain.

Brain tissue removal influences both components in equation (1): (i) the regularization in terms of the domain on which it is defined and (ii) the similarity in terms of additional outliers introduced due to resection. We extend the functional in equation (1) to equation (2) and we specify the regularization component in terms of a linear elastic strain energy:

$$\begin{aligned} u = \underset{u}{\operatorname{argmin}} (& \int_{\Omega - \Omega'} \sigma(u)^t \epsilon(u) d(\Omega - \Omega') + \\ & \lambda \sum_{s_i \in \Omega - \Omega'} \|s_i + u(s_i) - \sum_{t_j \in \Omega_R} c_{ij} t_j\|^2) \end{aligned} \quad (2)$$

where variable $\Omega^{'}$ represents the resected region and variable c_{ij} reflects the degree to which point s_i corresponds to t_j. c_{ij} is defined as in RPM [8], but we define a range Ω_R, a sphere centered at the source point with radius R, and only take into account: (1) the target points, which are located in Ω_R of the source point and (2) the source points, which have at least one target point in Ω_R. Therefore, unlike RPM, our method is capable of dealing with outliers existing in both point sets.

Remark In equation (2), if $\Omega^{'} = \varnothing$ and $c_{ij} = 1$ (see equation (4) for the calculation of c_{ij}), equation (2) is reduced to equation (1). This means our method can be viewed as a general point based NRR method.

We use finite element method to compute the numerical solution of equation (2):

$$W(U, C) = \sum_{E_i \in (M - M')} U^T K_{E_i} U + \lambda \|(HU - D(C))\|^2 \quad (3)$$

where C is the correspondence matrix with entries c_{ij}, the entries of the vector D are defined as: $d_i(c_{ij}) = s_i - \sum_{t_j \in \Omega_R} c_{ij} t_j, \forall s_i \in M - M'$, where M is the non-resected mesh that approximates Ω and $M^{'}$ is the resected mesh that approximates $\Omega^{'}$. The first term is the strain energy defined on all elements $E_i \in M - M'$ and the second term is similarity term defined for all source points $s_i \in M - M'$. U is node displacement, and H is interpolation matrix.

The difficulty to find U lies in the unsolved correspondence C, which is an outlier rejection problem. By extending the concept of the outliers from points to elements, the $M^{'}$ can be viewed as a collection of element outliers. Therefore, the problem for computing the three unknowns (*Correspondence*, *Deformation Field* and *Resection Region*) is reduced into a problem on: *How to reject point and element outliers*, where point outliers exist in both *Source* and *Target* sets and element outliers exist in the biomechanical model.

2.1. Feature Point Outlier Rejection

Assume M' is known, the more accurate estimation of C, the more accurate estimation of U and vice versa. Therefore, EM algorithm is employed to solve U and C under the specified M'. Unlike our previous work [10], which does not take resection into account, this method needs to be incorporated into a higher level EM along with the element rejection algorithm. For each source point s_i, assume its correspondences is subject to Gaussian distribution and c_{ij} can be calculated by equation (4).

$$c_{ij} = \frac{c'_{ij}}{\sum_{k=1}^{k=m} c'_{ik}}, c'_{ij} = \frac{1}{R\sqrt{2\pi}} e^{\frac{-(t_j - s_i)^2}{2R^2}}, \forall t_j \in \Omega_R, j = 1 \ldots m \quad (4)$$

Once C is estimated, U can be resolved using equation (3). Using this resolved U to warp S closer to T and then estimating the correspondence again will lead to EM algorithm, which is described as follows in Algorithm 1.

$[U, C]$=*PtOutlierRejection*(M, M', S, T)
Input: M: non-resected mesh, M': resected mesh,
S:source points,T:target points
Output: U: displacement vector, C: correspondence matrix
Initialize R and Tolerance ϵ
$U \Leftarrow I$
repeat
  Transform S based on U: $S \Leftarrow U(S)$
  E step:
    // outlier rejection for S
    $S \Leftarrow S - s_i$ if there are no target points in Ω_R for s_i
    // outlier rejection for T
    Estimate correspondence C according to equation 4
  M step:
    Solve U according to equation 3
  $error \Leftarrow \|U_i - U_{i-1}\|$ between successive iterations
  Decrease R
until $error < \epsilon$

Algorithm 1: Feature Point Outlier Rejection

2.2. Element Outlier Rejection

Assume the current deformation field and resection region is U and M' respectively, then the new estimated resection region can be obtained by transforming the remaining mesh $M - M'$ using U and then finding all elements, which are completely contained in the background image BGI and constitute the largest connected mesh with M'. BGI is a binary image with label 255 for background and 0 for non-background. It can be easily obtained using simple threshold segmentation method. To alleviate the influence to the regularization term induced by the element across the boundary, its biomechanical attribute (Young's modulus) will be scaled according to the percentage of non-background image in this element. This scaling will be clamped to 0.01 for the $percentage < 0.01$ to avoid arbitrary solution of the node in this element.

If we know U, the more accurate U is, the closer the deformed preoperative image will be to the intra-operative image, and therefore the more accurate the resected region will be (Note that the resected region has been deformed.). Inversely, the more accurate the resected region is, the more accurate U and C can be obtained using Alg. 1. As a result, the EM

$[M', S]$=*EleOutlierRejection*(M, M', U, BGI)

Input: M: non-resected mesh, M': resected mesh, U: displacement vector, BGI: background image

Output: M': new resected mesh, S: new source points

1: Obtain deformed remaining mesh $DM \Leftarrow U(M - M')$
2: Find all elements M_1 completely contained in the background image BGI and constitute the largest connected mesh with M'
3: Map M_1 in DM to M_2 in $M - M'$
4: $S \Leftarrow S - s_i, \forall s_i \in M_2$
5: $M' \Leftarrow M' + M_2$
6: Scale Young's modulus for the elements across the boundary

Algorithm 2: Element Outlier Rejection

Alg. 1 is embedded into a higher EM framework and proceeds as Alg. 3,

U=*FPBNRR*$(MRI, iMRI)$

Input: MRI: pre-operative MRI, $iMRI$: intra-operative MRI

Output: U: displacement vector

1: Segment brain on MRI and mesh generation for M
2: Segment background image BGI on $iMRI$
3: Canny edge detection on MRI to get S
4: Canny edge detection on $iMRI$ to get T
5: Initiate $M' \Leftarrow \varnothing$
6: **repeat**
7: M step: $U, C \Leftarrow$*PtOutlierRejection*(M, M', S, T)
8: E step: $M', S \Leftarrow$*EleOutlierRejection*(M, M', U, BGI)
9: **until** M' does not change

Algorithm 3: Feature Point Based NRR (FPBNRR)

3. RESULTS

We performed an evaluation based both on synthetic and real clinical data. We developed a tool to simulate brain resection. Fig. 1(a) depicts a snapshot from this tool. The source point set S is simulated as the mesh nodes of the surface shown as green color points in Fig. 1(b) and the target point set T is shown with white color points in Fig. 1(b). We evaluate algorithm *PtOutlierRejection*, for point outlier rejection, by considering all the surface nodes except the green color ones as the outliers (white color points in Fig. 1(c)) and add them into S. The outliers for T, are generated using white Gaussian noise and are depicted with green color in Fig. 1(d). The result shows that all the source points and target points are correctly detected and only three points (white color points in Fig. 1(e)) are not successfully rejected from over six thousand outliers. Fig. 1(f) shows the resulted target points, in which three white color points correspond to three non-rejected source points. Fig. 1(g) shows the remaining mesh $M - M'$ of algorithm *EleOutlierRejection*, where element outliers are correctly removed. A quick inspection on Fig 1(h) and Fig 1(i) depicts the improvement on the accuracy of our method. The result validates our hypothesis: accurate removal of the resected region can improve the accuracy of the registration result.

3.1. Clinical MRI Experiment

Fig. 2(a) and Fig. 2(b) depict a slice of 3D pre- and ROI in the intra-operative MRI, respectively. Fig. 2(c) depicts the discrepancy before FPBNRR registration. Specifically, it shows the

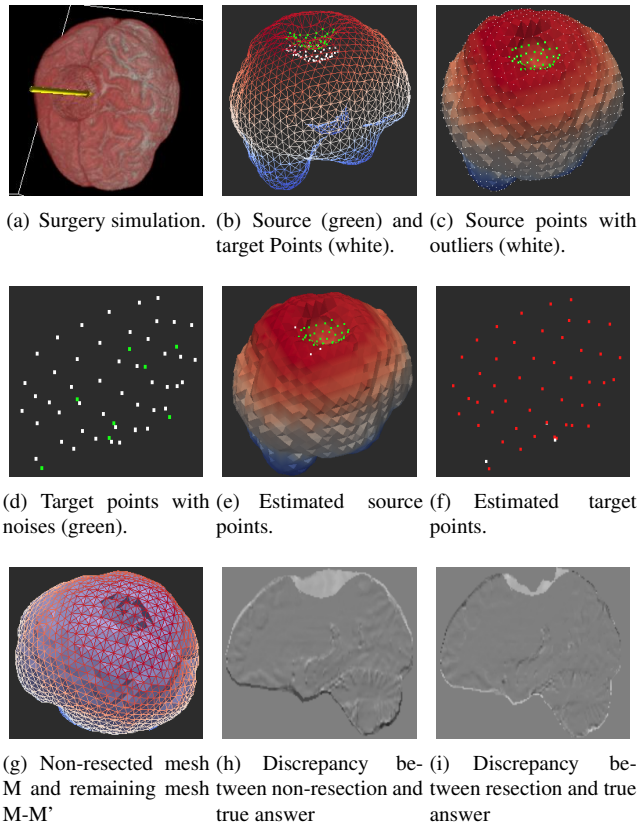

(a) Surgery simulation. (b) Source (green) and target Points (white). (c) Source points with outliers (white).

(d) Target points with noises (green). (e) Estimated source points. (f) Estimated target points.

(g) Non-resected mesh M and remaining mesh M-M' (h) Discrepancy between non-resection and true answer (i) Discrepancy between resection and true answer

Fig. 1. Results from the synthetic data.

boundary of (b) superimposed on (a) after rigid registration but before non-rigid registration.

The extracted boundary points on pre- and intra-operative MRI will be used as the source points (Fig. 2(a)) and target points (Fig. 2(c)) respectively. Both source points and target points are computed using ITK implementation of canny edge detection algorithm. After FPBNRR registration (see Fig. 2(d)), we observe: (i) the surface 1 is not deformed to outlier $1'$, which is not real brain surface, but the boundary of the ROI, (ii) the surface 2 still agrees well with the real boundary as it does before registration, although there are many outliers $2'$ around it, (iii) the surface 3 is correctly deformed to $3'$, (iv) however, the surface 8 is not affected by $8'$ due to outlier rejection and (v) the cavity 4 shows the resected region and 5 shows the remaining tumor. The comparison of another slice (92) is shown in Fig. 2(e) and Fig. 2(f). After registration, the surfaces of the ventricle on the deformed preoperative image matches well with that on intra-operative image. The surface 7 in the vicinity of the resection is also correctly deformed to $7'$.

In addition, Fig. 2(g), Fig. 2(h) and Fig. 2(i) are the results using the method (BMNRR) presented in [11]. This method uses Block Matching to find the correspondence and then drives the biomechanical model to estimate the deformation. Comparing Fig. 2(g) and Fig. 2(i) with Fig. 2(d) and Fig. 2(f) respectively (same slice as the number denotes), we can see the larger deformation in the vicinity of the tumor still exists after BMNRR. There are two reasons: (1) Block Matching cannot find correct correspondence near the resection region and (2) the resection region is not removed from biomechanical model. BMNRR shows as good results in the deep part of the brain as our method (see the ventricle in Fig. 2(h) and Fig. 2(i)) due to

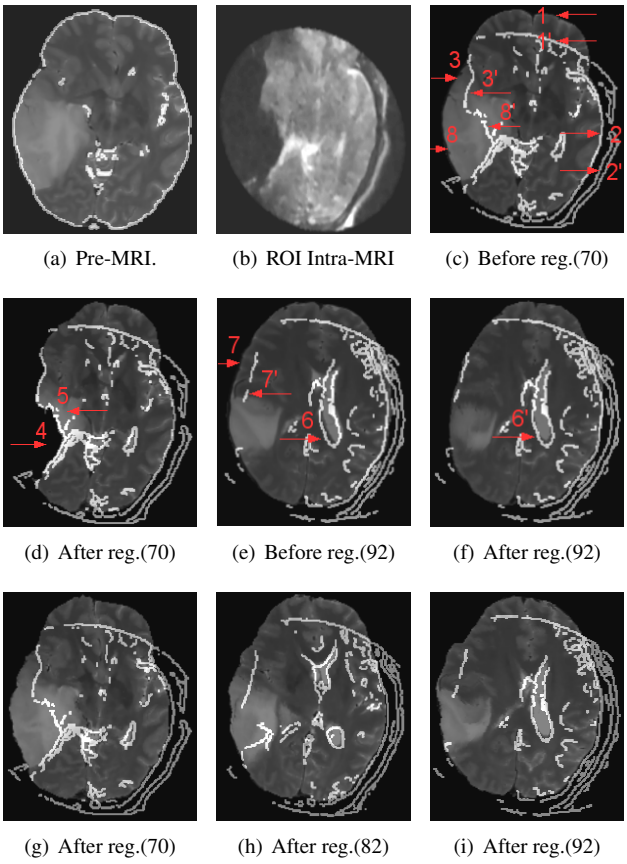

(a) Pre-MRI. (b) ROI Intra-MRI (c) Before reg.(70)

(d) After reg.(70) (e) Before reg.(92) (f) After reg.(92)

(g) After reg.(70) (h) After reg.(82) (i) After reg.(92)

Fig. 2. Results of FPBNRR.

fewer outliers and rich texture information, which are helpful for Block Matching.

In summary, our preliminary data shows that the new FPBNRR algorithm can handle iMRI with a resected region and incomplete data e.g. the brain region out of the ROI (see Fig. 2(b)) of low-field iMRI system. The resected region affects the regularization term, but the incomplete data does not. The FPBNRR method can successfully deal with the resection by using element rejection and incomplete data by using biomechanical model.

We quantitatively evaluate the result by using seven anatomical points on preoperative, intra-operative and deformed preoperative MRI respectively. For each point pair between pre- and intra-operative MRI, the magnitude of the displacement is calculated as the error before registration. For each pair between deformed pre- and intra-operative MRI, the magnitude is calculated as the error after registration. In these seven anatomical points, left and right anterior horn of lateral ventricle(LAH, RAH) are selected to evaluate the accuracy in the deep of the brain. Three right lateral fissure points (RLF1-3) are selected to evaluate the accuracy in the vicinity of the resection region. Two rigid points basilar sulcus (BS) and anterior commissure (AC) are selected to evaluate whether this method impairs the accuracy of these points, which we use for the rigid registration. Table 1 shows that after FPBNRR, the part near the resection region has higher accuracy compared to the deep part. The accuracy of the rigid registration points is affected slightly. BMNRR shows better accuracy in the deep part, but not in the vicinity of the tumor.

Table 1. Accuracy Evaluation (mm)

	Superficial points			Deep points		Rigid points	
Anatomical points	RLF1	RLF2	RLF3	LAH	RAH	BS	AC
Before registration	10.77	12.37	12.51	5.48	4.03	0.00	0.50
After FPBNRR	0.71	2.24	0.50	1.41	2.50	0.50	0.71
After BMNRR	15.52	14.23	11.10	2.29	1.73	0.00	0.50

4. CONCLUSION

We presented a novel point based non-rigid registration method, its implementation, and its evaluation using both synthetic and real clinical iMRI. The new method is very effective in registering pre-operative MRI with iMRI with brain tumor resection and it can be considered as a generalization of point based NRR. Our preliminary results show that the new method, in the vicinity of the tumor resection, for this specific case, is on average 16 times more accurate than rigid registration, and more accurate than the state-of-the-art NRR we used in clinical practice [1].

5. REFERENCES

[1] N. Archip, O. Clatz, A. Fedorov, A. Kot, S. Whalen, D. Kacher, N. Chrisochoides, F. Jolesz, A. Golby, P. Black, and S. K. Warfield, "Non-rigid alignment of preoperative mri, fmri, dt-mri, with intra-operative mri for enchanced visualization and navigation in image-guided neurosurgery," *Neuroimage*, vol. 35(2), pp. 609–624, 2007.

[2] S. Ding, M. I. Miga, J. H. Noble, A. Cao, P. Dumpuri, R. C. Thompson, and B. M. Dawant, "Semiautomatic registration of pre- and post brain tumor resection laser range data: method and validation," *IEEE Transactions on Biomedical Engineering*, vol. 56, no. 3, pp. 770–80, 2009.

[3] L. Vigneron, J. Verly, and S. Warfield, "Modelling surgical cuts, retractions, and resections via extended finite element method resections via extended finite element method," 09 2004.

[4] M. I. Miga, D.W. Roberts, F.E. Kennedy, L.A. Platenik, A. Hartov, K.E. Lunn, and K.D. Paulsen, "Modeling of retraction and resection for intraoperative updating of images," *Neurosurgery*, vol. 49, no. 1, pp. 75–84, 2001.

[5] A. P. Dempster, N. M. Laird, and D. B. Rubin, "Maximum likelihood from incomplete data via the em algorithm," *Journal of the Royal Statistical Society, Series B*, vol. 39, pp. 1–38, 1977.

[6] P. Risholm, E. Samset, I. Talos, and W. M. Wells III, "A non-rigid registration framework that accommodates resection and retraction," in *Inf Process Med Imaging IPMI 2009*, 2009, vol. 21, pp. 447–58.

[7] P. Risholm, E. L. Melvær, K. Mørken, and E. Samset, "Intraoperative adaptive fem-based registration accommodating tissue resection," in *Medical Imaging 2009: Image Processing*. 2009, vol. 7259, pp. 72592Y–72592Y–11, SPIE.

[8] C. Haili and A. Rangarajan, "A new point matching algorithm for non-rigid registration," *Comput. Vis. Image Underst.*, vol. 89, no. 2-3, pp. 114–141, 2003.

[9] S. Periaswamy and H. Farid, "Medical image registration with partial data," *Medical Image Analysis*, vol. 10, pp. 452–464, 2006.

[10] Y. Liu, A. Fedorov, R. Kikinis, and N. Chrisochoides, "A novel point based non-rigid registration method and its application on brain shift," in *SPIE Medical Imaging*, 2010, in proceeding.

[11] O. Clatz, H. Delingette, I.-F. Talos, A. Golby, R. Kikinis, F. Jolesz, N. Ayache, and S.K. Warfield, "Robust non-rigid registration to capture brain shift from intra-operative MRI," *IEEE Trans. Med. Imag.*, vol. 24, no. 11, pp. 1417–1427, 2005.